Lowest-order vertex-correction contribution to the direct gap of silicon

Lowest-order vertex-correction contribution to the direct gap of silicon

P. A. Bobbert and W. van Haeringen

Department of Physics, Eindhoven University of Technology, P.O. Box 513, 5600 MB Eindhoven, The Netherlands

(Received 29 October 1993)

We have calculated the contribution of the lowest-order vertex-correction diagram to the direct gap of silicon at the Γ-point, taking into account the dynamic screening of the electron-electron interaction. Our best calculation yields a contribution of 0.12 eV. This result supports the assumption of the GW approximation that vertex corrections can be neglected. We do not find a significant shift of the absolute energies.

I. INTRODUCTION

The GW approximation is one of the most successful approximations made in calculating the many-particle effects on the band structure of a variety of semiconductors and metals. The approximation amounts to replacing the infinite series of Feynman diagrams for the electron self-energy Σ by a single diagram Σ^{GW}, containing the full electron propagator G and the screened electron-electron interaction W (Fig. 1). The bare propagator G^0 is supposed to be the propagator of the electrons moving in the external ion potential plus the Hartree potential. G, G^0, and Σ are related to each other through the Dyson equation $G = G^0 + G^0 \Sigma G$. Neglected in the GW approximation are the so-called vertex corrections, of which the lowest-order diagram is also drawn in Fig. 1. This is the diagram on which we will focus our attention in this paper. We will henceforth call it Σ^{VC}.

Many GW calculations of the semiconductor silicon have been performed in recent years, of which we will only mention Refs. 1–3. One of the major difficulties in these calculations is that in the GW diagram in principle the exact G and W should be inserted, which of course are unavailable. One therefore uses the best known approximations, which for G usually means that one uses a local-density-approximation (LDA) propagator G^{LDA}, and for W a random-phase-approximation (RPA) screening with the LDA band structure and wave functions (an exception is Ref. 3, where band structures and wave functions obtained from an empirical pseudopotential method are used). To speed up the calculations, often a plasmon pole model[1,3] is used for the energy dependence of W, which works well for energies not too far (several eV) from the gap range. The band structure obtained with

FIG. 1. GW and lowest-order vertex-correction contribution to the self-energy. The screened interaction consists of the bare interaction v and a screening part W^{scr}.

such a procedure generally agrees within about 0.1 eV with the experimental band structure, when, e.g., the experimental and calculated valence-band maxima are aligned. In Ref. 2 it was noted that the GW valence-band maximum is about 0.5 eV below the accurate Ceperley-Alder[4] LDA-value. Since the density-functional-theory (DFT) energy for the valence-band maximum is exact [density-functional theory yields the correct ground state energies for the N- and $(N-1)$-electron systems], and since the local-density approximation is known to be a very good approximation of DFT in silicon, it was put forward in Ref. 2 that vertex corrections should leave relative energies unaltered, but should shift absolute energies upwards by about 0.5 eV.

Although the success of the GW approximation seems to prove that the vertex corrections, as far as energy differences are concerned, are indeed small in silicon, there is from a fundamental point of view still a need for an actual demonstration of this smallness. A very crude estimate of the lowest-order vertex-correction contribution to the direct gap of silicon was made by Bennett.[5] He employed Penn wave functions to construct the electron propagator G and used a screened static interaction for W. His result is a 65 meV correction to the direct gap (no result for the correction to the absolute energies was reported). A more sophisticated calculation was done in Ref. 6. In that paper the electron propagator was constructed from wave functions and energies obtained with an empirical pseudopotential method. Instead of the screened interaction W, the bare Coulomb interaction was used. The gap correction found was 47 meV with an uncertainty of about 100% (the correction to the absolute energies was about 0.2–0.3 eV). It was argued that the screening of the interaction could only decrease this number. A completely different approach was followed in Ref. 7. In the Hedin equation for the vertex function Γ, relating Γ to G and to the functional derivative of Σ with respect to G, Σ was approximated in that approach by the LDA exchange-correlation potential V_{xc} (in the original GW scheme[8] Σ was taken as zero in the Hedin equation for Γ). This leads to a "vertex correction" to W, as well as to Σ. This approach was called "$GW\Gamma$." The results obtained for the energy gaps with this method again agree within about 0.1 eV with experimental values and with the conventional GW approach. However, the valence-band maximum is now

hardly shifted (10 meV) with respect to the LDA value. Although these results are very encouraging, it is quite unclear which Feynman diagrams in the perturbation series of the self energy have been taken into account by such a procedure. In view of all this an estimate of the lowest-order vertex-correction contribution with dynamic screening effects fully included is desirable.

II. METHOD

We have evaluated the contribution $\Delta \epsilon^{\mathrm{VC}}$ of the vertex-correction diagram Σ^{VC} to the energies of the threefold-degenerate highest valence state Γ'_{25} and the threefold-degenerate lowest conduction state Γ_{15} at the Γ point ($\mathbf{k} = \mathbf{0}$) of Si by calculating

$$\Delta \epsilon_l^{\mathrm{VC}} = \hbar \langle \phi_{l,\mathbf{k}=\mathbf{0}} | \Sigma^{\mathrm{VC}}(\epsilon_l, \mathbf{k} = \mathbf{0}) | \phi_{l,\mathbf{k}=\mathbf{0}} \rangle. \qquad (1)$$

We used energies ϵ_l and wave functions $\phi_{l\mathbf{k}}(\mathbf{r})$ obtained from a LDA calculation. In Ref. 1 it was shown that the GW wave functions are practically indistinguishable from the LDA wave functions. The GW energies, however, differ appreciably from the LDA energies. To estimate the effect of taking the GW energies in Eq. (1) instead of the LDA energies, we also calculated

$$\delta_l^{\mathrm{VC}} = \hbar \langle \phi_{l,\mathbf{k}=\mathbf{0}} | \left. \frac{\partial \Sigma^{\mathrm{VC}}(\epsilon, \mathbf{k} = \mathbf{0})}{\partial \epsilon} \right|_{\epsilon=\epsilon_l} | \phi_{l,\mathbf{k}=\mathbf{0}} \rangle. \qquad (2)$$

We used the LDA electron propagator for G in the vertex-correction diagram. We started from a LDA calculation with a plane wave basis having an energy cutoff of 11.2 Ry. The *ab initio* ion potential of Ref. 9 was used.

The static screened interaction W for $\epsilon = 0$ was calculated with a RPA dielectric constant and its energy dependence was modeled with the plasmon pole model of Engel and Farid.[10] This model is superior to the plasmon pole models used in Refs. 1 and 3 in that the plasmon bands have a clear physical interpretation. In Ref. 10, the authors also show that the energy dependence of some important elements of the inverse dielectric matrix resulting from the full RPA calculation is reproduced better by their own plasmon pole model than by the plasmon pole model of Hybertsen and Louie.[1] Of crucial importance for our purpose, however, is the fact that by using this model some of the reciprocal lattice sums in the expression for Σ^{VC} decouple, which is essential for making our calculations feasible. In Appendix A we briefly review this plasmon pole model. The plasmon pole model allows us to perform the two energy integrations occurring in the vertex-correction diagram analytically.

We can write the screened interaction as a sum of the bare Coulomb interaction v and a screening part W^{scr} (see also Fig. 1). When we now split up the vertex-correction diagram into subdiagrams according to the specific time order of the four vertices and according to the number of occurrences of the screening part W^{scr}, we get in total 38 different possibilities. These subdiagrams are shown in Fig. 2 and classified into 16 classes. Each of these diagrams contains two Brillouin zone in-

tegrations over the momenta $\mathbf{q}_1$ and $\mathbf{q}_2$ exchanged at the internal vertices. These two integrations were replaced by discrete sums over the $(2N)^3$ points of the grid $\mathbf{q} = (n_1 \mathbf{b}_1 + n_2 \mathbf{b}_2 + n_3 \mathbf{b}_3)/(2N)$ $(n_i = -N + 1, \cdots, N$, with $\mathbf{q}$ reduced to the first Brillouin zone if necessary), where $\mathbf{b}_1$, $\mathbf{b}_2$, and $\mathbf{b}_3$ are the primitive vectors of the bcc reciprocal lattice of Si. When the points of this grid are transformed to the irreducible wedge by point group transformations, only 8, 16, 30, 48, 74 different points remain for $N = 2, 3, 4, 5, 6$. Because Σ^{VC} is evaluated at $\mathbf{k} = \mathbf{0}$ one of the momentum integrations can be restricted to the irreducible wedge, whereas the other integration should be performed over the whole Brillouin zone. The integrand of each class of diagrams in Fig. 2, when sandwiched between the Γ'_{25} or Γ_{15} LDA wave functions, has its particular singularity when $\mathbf{q}_1 \to \mathbf{0}$ or $\mathbf{q}_2 \to \mathbf{0}$. These singularities are all integrable and are handled analytically in a way similar to that described in Appendix B of Ref. 6. As an example, for the diagram CVVS the expression obtained for Σ^{VC} is worked out in Appendix B.

The integrands of the diagrams CVC, all of the diagrams contributing to CVCS, and all of the diagrams but the last contributing to CVCSS, contain an energy
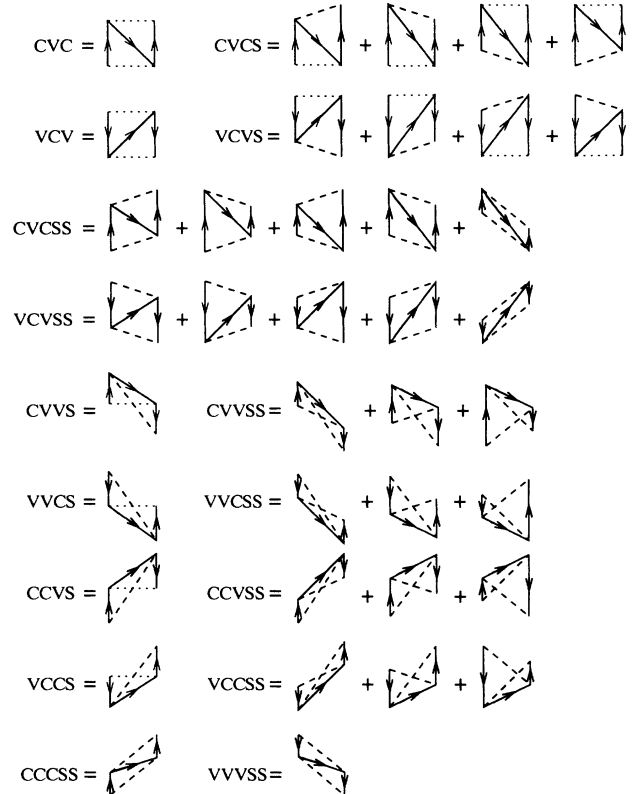
FIG. 2. Classification of the 38 subdiagrams contributing to the vertex-correction diagram. A directed line stands for an electron propagator, a dotted line for the bare Coulomb interaction, and a dashed line for the screening part of the screened interaction. Time increases from bottom to top. "C" and "V" stand for the conduction-band and valence-band parts of the electron propagator respectively and "S" stands for the screening part of the interaction.

denominator $\epsilon - \epsilon_{l_1}(\mathbf{q}_1) + \epsilon_{l_2}(\mathbf{q}_1 + \mathbf{q}_2) - \epsilon_{l_3}(\mathbf{q}_2)$, where l_1 and l_3 are conduction-band indices and l_2 a valence-band index (see the caption of Fig. 2 for an explanation of the names of these diagrams). If ϵ is the energy of Γ_{15} (lowest conduction state at the Γ point), there is a region in $1\mathrm{BZ} \times 1\mathrm{BZ}$ where this denominator can become zero (this is because in the LDA band structure the energy difference between the energy of Γ_{15} and the energy of the lowest conduction state is larger than the indirect gap energy). However, on the grids used for the Brillouin zone integrations this energy denominator never became smaller than 0.2 eV and caused no problems in the calculation of $\Delta\epsilon^{\mathrm{VC}}$ for Γ_{15}.

III. RESULTS AND DISCUSSION

For the most accurate calculation[11] performed, the contributions to $\Delta\epsilon^{\mathrm{VC}}$ of the different classes of diagrams are tabulated in Table I. For the grid used for the Brillouin zone integrations we took $N = 3$ (216×216 points in $1\mathrm{BZ} \times 1\mathrm{BZ}$). The number of plane waves taken into account in all the reciprocal lattice vector summations was $N_{\mathrm{PW}} = 137$. The number of electron and plasmon bands taken into account was $N_{\mathrm{band}} = 65$. These numbers are comparable to the ones used in Ref. 1. The results are $\Delta\epsilon^{\mathrm{VC}} = -0.089$ and 0.033 eV for Γ'_{25} and Γ_{15}, respectively. Hence, we find a gap correction of 0.122 eV.

With the same cutoffs and grid we calculated the energy contribution of the GW diagram to several valence and conduction states, incorporating the contribution due to the energy derivative at the LDA energies. The results for the direct band gaps at the Γ, L, and X points are 3.31 eV, 3.33 eV, and 4.20 eV, respectively. These values are quite comparable to those of, e.g., Hybertsen and Louie[1] (3.35 eV, 3.54 eV, and 4.43 eV). Experimental values are 3.40 eV, 3.45 eV,[12] and 4.25 eV.[13] The contribution of the lowest-order vertex correction leads to a direct gap at Γ which is also in good agreement with the experimental value (we do not want to attach too much value to the fact that the agreement seems even better now, since there are still uncertainties of the order of 0.1 eV due to several approximations, e.g. the fact that the LDA propagator is not the exact one).

With a coarser grid ($N = 2$) we find for the lowest-order vertex-correction contribution $\Delta\epsilon^{\mathrm{VC}} = -0.126$ and

0.106 eV for Γ'_{25} and Γ_{15}, respectively. Taking into account fewer plane waves ($N_{\mathrm{PW}} = 89$) or more bands ($N_{\mathrm{band}} = 89$) these latter numbers changed by only a few hundredth of an eV. Since the gap correction calculated with the coarser ($N = 2$) grid is larger than that calculated with the finer ($N = 3$) grid, we expect the value of 0.12 eV to be an upper bound. Calculations with an even finer grid ($N = 4$) were beyond the computational reach.

The results of the $N = 3$, $N_{\mathrm{PW}} = 137$, and $N_{\mathrm{band}} = 65$ calculation for δ^{VC} [Eq. (2)] are -0.066 and -0.051 for Γ'_{25} and Γ_{15}, respectively. Considering the fact that the GW energies are shifted with respect to the LDA energies by typically a few tenths of an eV, the first-order correction of $\Delta\epsilon^{\mathrm{VC}}$, related to the energy derivative of Σ^{VC}, is minute. We also calculated the vertex correction to the energy of the second-lowest conduction state Γ'_2: $\Delta\epsilon^{\mathrm{VC}} = -0.045$ eV and $\delta^{\mathrm{VC}} = -0.048$. These values are in line with the values reported above. For the lowest valence state Γ_1 we were not able to calculate reliable values, because of frequent occurrences of small energy denominators.

A remarkable fact is that the smallness of $\Delta\epsilon^{\mathrm{VC}}$ is not a result of systematic cancellations among the different classes of diagrams in Table I. It is true that contributions of diagrams which can be obtained from each other by reversing the time order are of opposite sign, but the cancellation is far from complete. Only when adding up *all* contributions do we get small numbers. It therefore seems dangerous to make general predictions about the size of $\Delta\epsilon^{\mathrm{VC}}$ for other materials.

We can check the assertion of Ref. 6 that screening effects will decrease the contributions of the diagrams CVC and VCV. From Table I we see that the CVC diagram yields an energy correction of 1.590 and 1.454 eV to Γ'_{25} and Γ_{15}, respectively. Screening one interaction (CVC+CVCS) these numbers change to 0.500 and 0.500 eV. Screening both interactions (CVC+CVCS+CVCSS) we get 0.722 and 0.658 eV. For the time-reversed diagrams these numbers are -0.826 and -0.765 eV (VCV), -0.316 and -0.119 eV (VCV+VCVS), -0.355 and -0.269 eV (VCV+VCVS+VCVSS). Hence, screening effects *do* decrease the contributions of the diagrams CVC and VCV to the energy corrections of Γ'_{25} and Γ_{15}, but only with a factor of roughly 0.5. The effect on the contribution to the gap is less systematic: it changes from

TABLE I. Lowest-order vertex-correction contribution $\Delta\epsilon^{\mathrm{VC}}$ in eV to the energies of Γ'_{25} and Γ_{15} (highest valence state and lowest conduction state at $\mathbf{k} = 0$) of Si. The different classes of diagrams are indicated in Fig. 2.

|	CVC	CVCS	CVCSS	VCCS+CCVS	VCCSS+CCVSS	CCCSS	Total
Γ'_{25}	1.590	−1.090	0.222	−1.641	0.797	−0.116	−0.238
Γ_{15}	1.454	−0.954	0.158	−0.670	0.264	−0.363	−0.111
	VCV	VCVS	VCVSS	CVVS+VVCS	CVVSS+VVCSS	VVVSS	Total
Γ'_{25}	−0.826	0.510	−0.039	0.509	−0.211	0.206	0.149
Γ_{15}	−0.765	0.646	−0.150	0.804	−0.416	0.025	0.144
	Total	Total	Total	Total	Total	Total	Total
Γ'_{25}	0.764	−0.580	0.183	−1.132	0.586	0.090	−0.089
Γ_{15}	0.689	−0.308	0.008	0.134	−0.152	−0.338	0.033
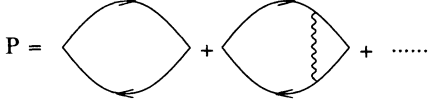
FIG. 3. RPA approximation of the irreducible polarization P and its lowest-order vertex correction.

-0.136 (CVC) and 0.061 eV (VCV) for the unscreened diagrams to -0.064 (CVC+CVCS+CVCSS) and 0.086 eV (VCV+VCVS+VCVSS) for the fully screened diagrams.

The most surprising result in Table I, however, is the large contribution of the diagrams in which at least two subsequent fermion lines are of either the type C or V (see Fig. 2). Such diagrams can only exist due to the noninstantaneous character of the screened interaction W. The reason for the unexpectedly large contribution of these diagrams can be traced back to the fact that for these diagrams at one or both of the internal vertices an electron or hole can come in and go out *in the same band*. When the momentum carried by the interaction line connected to such a vertex approaches zero, we end up with an inner product between states with the same Bloch vector. This inner product is zero if these states are in different bands, but unity if they are equal (see the example in Appendix B). These diagrams were not accounted for in Ref. 6 nor in Ref. 5.

Our calculations do not yield the 0.5 eV energy shift, predicted in Ref. 2. One possible reason for this could be that the screened interaction is calculated with a RPA dielectric constant. This could be checked by also calculating the lowest-order vertex correction to the irreducible polarizability P (see Fig. 3). Unfortunately, this would produce an even more difficult numerical task. However, according to the calculations of Ref. 7 it is not the vertex correction of W which causes the energy shift (this correction even leads to a small *decrease* of the energies), but the vertex correction of Σ. This inevitably seems to lead to the conclusion that *higher-order* vertex corrections are responsible for the energy shift.

Having established the smallness of the contribution of the lowest-order vertex-correction diagram to the direct gap, it still has to be realized that there is no *a priori* guarantee that the total contribution of all vertex-correction diagrams is also small.

APPENDIX A

In Ref. 10 the energy-dependent screened interaction $W^{\mathrm{scr}}_{\mathbf{K}_1,\mathbf{K}_2}(\mathbf{k},\epsilon)$ in a plane wave basis ($\mathbf{K}_i$ is a reciprocal lattice vector) is written as

$$W_{\mathbf{K}_1,\mathbf{K}_2}(\mathbf{k},\epsilon) = v_{\mathbf{K}_1,\mathbf{K}_2}(\mathbf{k}) + W^{\mathrm{scr}}_{\mathbf{K}_1,\mathbf{K}_2}(\mathbf{k},\epsilon), \qquad (\mathrm{A1})$$

where $v_{\mathbf{K}_1,\mathbf{K}_2}(\mathbf{k})$ is the bare Coulomb interaction

$$v_{\mathbf{K}_1,\mathbf{K}_2}(\mathbf{k}) = \frac{e^2}{\epsilon_0|\mathbf{k}+\mathbf{K}_1|^2}\delta_{\mathbf{K}_1,\mathbf{K}_2}. \qquad (\mathrm{A2})$$

For $W^{\mathrm{scr}}_{\mathbf{K}_1,\mathbf{K}_2}(\mathbf{k},\epsilon)$ the following plasmon pole model is derived:

$$W^{\mathrm{scr}}_{\mathbf{K}_1,\mathbf{K}_2}(\mathbf{k},\epsilon) = \sum_m \left(\frac{1}{\epsilon - \omega_m(\mathbf{k}) + i\eta} - \frac{1}{\epsilon + \omega_m(\mathbf{k}) - i\eta} \right)$$
$$\times w_{m\mathbf{k}}(\mathbf{K}_1)w^*_{m\mathbf{k}}(\mathbf{K}_2), \qquad (\mathrm{A3})$$

where η is a small positive energy. The plasmon pole energies $\omega_m(\mathbf{k})$ and the coefficients $w_{m\mathbf{k}}(\mathbf{K})$ of the plasmon functions in this expression can be related to the following generalized eigenvalue problem:

$$\underline{\chi}(\mathbf{k},\epsilon=0)\vec{x}_{m\mathbf{k}} = -\frac{1}{\omega^2_m(\mathbf{k})}\underline{M}(\mathbf{k})\vec{x}_{m\mathbf{k}}. \qquad (\mathrm{A4})$$

Here the shorthand notations $\underline{A}$ for matrices $A_{\mathbf{K}_1,\mathbf{K}_2}$ and $\vec{x}$ for vectors $x_\mathbf{K}$ were adopted. In Eq. (A4), $\underline{\chi}(\mathbf{k},\epsilon=0)$ is the full polarizability at zero energy. The full polarizability at complex energy z is related to the irreducible polarizability $\underline{P}(\mathbf{k},z)$ by

$$\underline{\chi}(\mathbf{k},z) = \underline{P}(\mathbf{k},z)\left[\underline{I} - \underline{v}(\mathbf{k})\underline{P}(\mathbf{k},z)\right]^{-1}, \qquad (\mathrm{A5})$$

with $\underline{I}$ the unit matrix. The RPA expression for $\underline{P}(\mathbf{k},z)$ is:[14,15]

$$P_{\mathbf{K}_1,\mathbf{K}_2}(\mathbf{k},z) = \frac{2}{(2\pi)^3}\int_{1\mathrm{BZ}} d^3q \left(\sum_{l_1\in\mathrm{CB}}\sum_{l_2\in\mathrm{VB}} - \sum_{l_1\in\mathrm{VB}}\sum_{l_2\in\mathrm{CB}} \right) \frac{1}{z - \epsilon_{l_1}(\mathbf{q}) + \epsilon_{l_2}(\mathbf{q}-\mathbf{k})}$$

$$\times \left(\sum_Q d_{l_1\mathbf{q}}(\mathbf{Q})d^*_{l_2\mathbf{q}-\mathbf{k}}(\mathbf{Q}-\mathbf{K}_1) \right) \left(\sum_Q d^*_{l_1\mathbf{q}}(\mathbf{Q})d_{l_2\mathbf{q}-\mathbf{k}}(\mathbf{Q}-\mathbf{K}_2) \right). \qquad (\mathrm{A6})$$

In this expression $\epsilon_l(\mathbf{k})$ is a band energy (CB stands for conduction-band and VB for valence-band index) and $d_{l\mathbf{k}}(\mathbf{K})$ are the plane wave coefficients of the wave function $\phi_{l\mathbf{k}}$ with wave vector $\mathbf{k}$ and band index l:

$$\phi_{l\mathbf{k}}(\mathbf{r}) = \frac{1}{\sqrt{\Omega}}\sum_\mathbf{K} d_{l\mathbf{k}}(\mathbf{K})e^{i(\mathbf{k}+\mathbf{K})\cdot\mathbf{r}}, \qquad (\mathrm{A7})$$

with Ω the crystal volume.

The matrix $\underline{M}(\mathbf{k})$ in Eq. (A4) is related to the plane wave coefficients of the density $\rho(\mathbf{K})$ through

$$M_{\mathbf{K}_1,\mathbf{K}_2}(\mathbf{k}) = \frac{\hbar^2}{m_e}(\mathbf{k} + \mathbf{K}_1) \cdot (\mathbf{k} + \mathbf{K}_2)\rho(\mathbf{K} - \mathbf{K}'), \quad \text{(A8)}$$

with m_e the electronic mass. It can be shown that the matrix $\underline{\chi}(\mathbf{k}, z = 0)$ is Hermitian and negative definite, whereas $\underline{M}(\mathbf{k})$ is Hermitian and positive definite. Hence, the eigenvalues $\omega_m^2(\mathbf{k})$ are real and positive. The eigenvectors $\vec{x}_{m\mathbf{k}}$ should be normalized according to

$$\vec{x}_{m\mathbf{k}}^\dagger \underline{M}(\mathbf{k})\vec{x}_{n\mathbf{k}} = \delta_{m,n}, \quad \text{(A9)}$$

and satisfy the completeness relation

$$\sum_m \vec{x}_{m\mathbf{k}}\vec{x}_{m\mathbf{k}}^\dagger = \underline{M}^{-1}(\mathbf{k}). \quad \text{(A10)}$$

The coefficients $w_{m\mathbf{k}}(\mathbf{K})$ in Eq. (A3) are related to the eigenvectors $x_{m\mathbf{k}}(\mathbf{K})$ of Eq. (A4) by

$$\vec{w}_{m\mathbf{k}} = \frac{1}{\sqrt{2\omega_m(\mathbf{k})}}\underline{v}(\mathbf{k})\underline{M}(\mathbf{k})\vec{x}_{m\mathbf{k}}. \quad \text{(A11)}$$

APPENDIX B

The general expression for Σ^{VC} is

$$\Sigma_{\mathbf{K}_1,\mathbf{K}_2}^{\mathrm{VC}}(\mathbf{k}, \epsilon) = -\frac{1}{(2\pi)^8\hbar^4}\int_{\mathrm{1BZ}} d^3q_1 \int_{\mathrm{1BZ}} d^3q_2 \int_{-\infty}^{\infty} d\epsilon_1 \int_{-\infty}^{\infty} d\epsilon_2 \sum_{\mathbf{Q}_1\cdots\mathbf{Q}_6} G_{\mathbf{Q}_4,\mathbf{K}_2-\mathbf{Q}_2}(\mathbf{q}_1, \epsilon_1)$$

$$\times G_{\mathbf{Q}_3-\mathbf{Q}_5,\mathbf{Q}_4-\mathbf{Q}_6}(\mathbf{q}_1 + \mathbf{q}_2 - \mathbf{k}, \epsilon_1 + \epsilon_2 - \epsilon)G_{\mathbf{K}_1-\mathbf{Q}_1,\mathbf{Q}_3}(\mathbf{q}_2, \epsilon_2)$$

$$\times W_{\mathbf{Q}_5,\mathbf{Q}_2}(\mathbf{k} - \mathbf{q}_1, \epsilon_1 - \epsilon)W_{\mathbf{Q}_1,\mathbf{Q}_6}(\mathbf{k} - \mathbf{q}_2, \epsilon_2 - \epsilon). \quad \text{(B1)}$$

The Lehmann representation for the noninteracting LDA electron propagator G^{LDA} is:[16]

$$G_{\mathbf{K}_1,\mathbf{K}_2}^{\mathrm{LDA}}(\mathbf{k}, \epsilon) = \hbar\sum_l \frac{d_{l\mathbf{k}}(\mathbf{K}_1)d_{l\mathbf{k}}^*(\mathbf{K}_2)}{\epsilon - \epsilon_l(\mathbf{k}) + i\eta\,\mathrm{sgn}[\epsilon_l(\mathbf{k}) - \mu]}, \quad \text{(B2)}$$

with μ the chemical potential. Inserting Eq. (B2) into Eq. (B1) and using the plasmon pole model Eq. (A3) for W given in Appendix A, the ϵ_1 and ϵ_2 integrations can be performed analytically with contour integration. For each of the 38 diagrams in Fig. 2 one obtains a different expression. It is of no use to give all these expressions here, because this would fill several pages and because the derivations are straightforward. As an example we will give the expression for the contribution of the diagram CVVS (see Fig. 2) to $\Delta\epsilon^{\mathrm{VC}}$ [Eq. (1)] of the wave function with band index l at $\mathbf{k} = \mathbf{0}$:

$$\Delta\epsilon_l^{\mathrm{CVVS}} = \hbar\langle\phi_{l,\mathbf{k}=\mathbf{0}}|\Sigma^{\mathrm{CVVS}}(\epsilon_l, \mathbf{k} = \mathbf{0})|\phi_{l,\mathbf{k}=\mathbf{0}}\rangle$$

$$= -\frac{e^2}{\epsilon_0(2\pi)^6}\int_{\mathrm{1BZ}} d^3q_1 \int_{\mathrm{1BZ}} d^3q_2$$

$$\times \sum_{l_1\in\mathrm{CB}}\sum_{l_2\in\mathrm{VB}}\sum_{l_3\in\mathrm{VB}}\sum_m \frac{1}{[\epsilon_{l_1}(\mathbf{q}_1) - \epsilon_{l_2}(\mathbf{q}_1 + \mathbf{q}_2) + \omega_m(\mathbf{q}_2)][\epsilon_l(\mathbf{k} = \mathbf{0}) - \epsilon_{l_3}(\mathbf{q}_2) + \omega_m(\mathbf{q}_2)]}$$

$$\times \sum_{\mathbf{K}_2,\mathbf{Q}_2} \frac{d_{l,\mathbf{k}=\mathbf{0}}(\mathbf{K}_2)d_{l_1\mathbf{q}_1}^*(\mathbf{K}_2 - \mathbf{Q}_2)}{|\mathbf{q}_1 - \mathbf{Q}_2|^2}\sum_{\mathbf{Q}_3} d_{l_3\mathbf{q}_2}^*(\mathbf{Q}_3)d_{l_2\mathbf{q}_1+\mathbf{q}_2}(\mathbf{Q}_3 - \mathbf{Q}_2)$$

$$\times \sum_{\mathbf{K}_1,\mathbf{Q}_1} d_{l,\mathbf{k}=\mathbf{0}}^*(\mathbf{K}_1)d_{l_3\mathbf{q}_2}(\mathbf{K}_1 - \mathbf{Q}_1)w_{m,-\mathbf{q}_2}(\mathbf{Q}_1)$$

$$\times \sum_{\mathbf{Q}_4,\mathbf{Q}_6} w_{m,-\mathbf{q}_2}^*(\mathbf{Q}_6)d_{l_1\mathbf{q}_1}(\mathbf{Q}_4)d_{l_2\mathbf{q}_1+\mathbf{q}_2}^*(\mathbf{Q}_4 - \mathbf{Q}_6). \quad \text{(B3)}$$

The advantage of using the plasmon pole model of Ref. 10 instead of that of Ref. 1 is clear: the $\mathbf{Q}_1$ and $\mathbf{Q}_6$ summations in the above expression can be performed independently.

If $l \in \mathrm{CB}$, the $\mathbf{Q}_2 = \mathbf{0}$ term of the expression Eq. (B3) diverges like $1/|\mathbf{q}_1|^2$ when $\mathbf{q}_1 \to 0$. The reason for this is that for $\mathbf{Q}_2 = 0$, $l_1 = l$, $l_3 = l_2$, and $\mathbf{q}_1 \to 0$ we have twice an inner product of a wave function with itself, which is unity. For $l \in \mathrm{CB}$ the expression Eq. (B3) remains finite, however, when $\mathbf{q}_2 \to 0$, because the $1/|\mathbf{q}_2|$ divergences of

$w_{m,-\mathbf{q}_2}(\mathbf{Q}_1)$ for $\mathbf{Q}_1 = 0$ and of $w_{m,-\mathbf{q}_2}^*(\mathbf{Q}_6)$ for $\mathbf{Q}_6 = 0$ are canceled by two factors of the form

$$\sum_{\mathbf{K}} d_{l_1\mathbf{q}_1}^*(\mathbf{K})d_{l_2\mathbf{q}_1+\mathbf{q}_2}(\mathbf{K}) \equiv \mathbf{B}_{l_1,l_2}(\mathbf{q}_1) \cdot \mathbf{q}_2, \quad \text{(B4)}$$

if $\mathbf{q}_2 \to 0$ and $l_1 \neq l_2$. If $l \in \mathrm{VB}$, the expression Eq. (B3) diverges like $\mathbf{B} \cdot \mathbf{q}_1/|\mathbf{q}_1|^2$ when $\mathbf{q}_1 \to 0$ and like $1/|\mathbf{q}_2|$ when $\mathbf{q}_2 \to 0$. The contribution of the diagram CVVS to δ^{VC} is simply obtained by multiplying the integrand of Eq. (B3) by $-[\epsilon_l(\mathbf{k} = \mathbf{0}) - \epsilon_{l_3}(\mathbf{q}_2) + \omega_m(\mathbf{q}_2)]^{-1}$.

[1] M.S. Hybertsen and S.G. Louie, Phys. Rev. B **34**, 5390 (1986).

[2] R.W. Godby, M. Schlüter, and L.J. Sham, Phys. Rev. B **37**, 10 159 (1988).

[3] W.v.d. Linden and P. Horsch, Phys. Rev. B **37**, 8351 (1988).

[4] D.M. Ceperley and B.I. Alder, Phys. Rev. Lett. **45**, 566 (1980); parametrized in J.P. Perdew and A. Zunger, Phys. Rev. B **23**, 5048 (1981).

[5] M. Bennett, J. Phys. C **11**, L515 (1978).

[6] R. Daling and W. van Haeringen, Phys. Rev. B **40**, 11 659 (1989).

[7] R. Del Sole, L. Reining, and R.W. Godby, Phys. Rev. B (to be published).

[8] L. Hedin, Phys. Rev. **139**, A796 (1965).

[9] G.B. Bachelet, H.S. Greenside, G.A. Baraff, and M. Schlüter, Phys. Rev. B **24**, 4745 (1981).

[10] G.E. Engel and B. Farid, Phys. Rev. B **47**, 15 931 (1993).

[11] This calculation was performed on IBM RS/6000 computers (models 320 and 220) and took approximately 700 hours of CPU time.

[12] *Physics of Group-IV Elements and III-V Compounds*, edited by O. Madelung, M. Schulz, and H. Weiss, Landolt-Börnstein, New Series (Springer, New York, 1982) Group III, Vol. 17, Pt. a.

[13] D.E. Aspnes and A.A. Studna, Phys. Rev. B **27**, 985 (1983).

[14] S.L. Adler, Phys. Rev. **126**, 413 (1962).

[15] N. Wiser, Phys. Rev. **129**, 62 (1963).

[16] A.L. Fetter and J.D. Walecka, *Quantum Theory of Many-Particle Systems* (McGraw-Hill, New York, 1971), Chap. 3.